THE JOURNAL OF BIOLOGICAL CHEMISTRY
Vol. 275, No. 44, Issue of November 3, pp. 34557–34565, 2000

Printed in U.S.A.

Crystal Structure of 1-Aminocyclopropane-1-carboxylate Deaminase from *Hansenula saturnus**

Received for publication, May 31, 2000, and in revised form, August 6, 2000
Published, JBC Papers in Press, August 10, 2000, DOI 10.1074/jbc.M004681200

Min Yao‡, T. Ose‡, Hiroshi Sugimoto‡, Atsushi Horiuchi‡, Atsushi Nakagawa‡§, Soichi Wakatsuki¶, Daisuke Yokoi‖, Toyotaka Murakami‖, Mamoru Honma‖, and Isao Tanaka‡§**

From the ‡Graduate School of Science, Hokkaido University, Sapporo 060-0810, Japan, the ‖Graduate School of Agriculture, Hokkaido University, Sapporo 060-8589, Japan, and the ¶European Synchrotron Radiation Facility, BP 220, F-38043 Grenoble Cedex, France

The pyridoxal 5′-phosphate (PLP)-dependent enzyme 1-aminocyclopropane-1-carboxylate deaminase (ACCD) catalyzes a reaction that involves a ring opening of cyclopropanoid amino acid, yielding α-ketobutyrate and ammonia. Unlike other PLP-dependent enzymes, this enzyme has no α-hydrogen atom in the substrate. Thus, a unique mechanism for the bond cleavage is expected. The crystal structure of ACCD from *Hansenula saturnus* has been determined at 2.0 Å resolution by the multiple wavelength anomalous diffraction method using mercury atoms as anomalous scatterers. The model was built on the electron density map, which was obtained by the density averaging of multiple crystal forms. The final model was refined to an *R*-factor of 22.5% and an R_{free}-factor of 26.8%. The ACCD folds into two domains, each of which has an open twisted α/β structure similar to the β-subunit of tryptophan synthase. However, in ACCD, unlike in other members of the β family of PLP-dependent enzymes, PLP is buried deep in the molecule. The structure provides the first view of the catalytic center of the cyclopropane ring opening.

A pyridoxal 5′-phosphate (PLP)[1]-dependent enzyme, 1-aminocyclopropane-1-carboxylate deaminase (ACCD), was originally found in a soil bacterium *Pseudomonas* sp. strain ACP as an enzyme that degrades a cyclopropanoid amino acid 1-aminocyclopropane-1-carboxylic acid (ACC) to α-ketobutyrate and ammonia (1) (Fig. 1). ACC is known to be a key intermediate in the biosynthesis of a plant hormone ethylene that affects diverse growth and fruit ripening (2). In higher plants, ethylene biosynthesis starts with the *S*-adenosylation of methionine in order to give *S*-adenosylmethionine. This step is followed by the closing a cyclopropane ring to form ACC, which is then oxidatively cleaved to give ethylene (3). The introduction of ACCD in higher plants by gene technology reduces the production level of ethylene and delays the ripening progression of fruits (4, 5). Thus, this enzyme provides a way to regulate ethylene biosynthesis and plant ripening.

PLP-dependent enzymes catalyze many important reactions that act upon amino acids, including transamination, decarboxylation, β,γ-replacement/elimination, and racemization (6, 7). In all of these reactions (except in the case of the glycogen phosphorylase family), the two basic chemical properties of the PLP are conserved; it forms an external aldimine between its aldehyde group and the α-amino group of the substrates and withdraws electrons from the substrate by serving as an electron sink (7). As a PLP-dependent enzyme, the ACCD's ring-opening reaction starts with a transformation reaction from an internal aldimine between the PLP and the enzyme to an external aldimine. In most of the PLP-dependent enzymes, the next step is the nucleophilic abstraction of the α-substituent, either an α-proton or a carboxylate group, to form an α-carbanionic intermediate. This reaction mechanism cannot be applied to ACCD because the substrate (ACC) does not contain α-hydrogen and the carboxyl group is retained in the product. Therefore, the ring-opening reaction of ACC must be initiated without obvious accessibility to an α-carbanionic intermediate, which is, for PLP-dependent enzymes, the common entry for catalysis. One proposed reaction mechanism is the nucleophilic addition to C_γ followed by the cleavage of the C_α-C_γ bond and β-proton abstraction. Because PLP acts as an electron sink, external aldimine is fairly electrophilic, and the nucleophilic addition to C_γ to rupture the cyclopropane ring of ACC is mechanistically feasible (8, 9).

To understand such a reaction mechanism on a molecular basis, a knowledge of the three-dimensional structure of the enzyme is necessary. The ACC deaminases from the bacterium *Pseudomonas* sp. (bACCD; EC 4.1.99.4) and the yeast *Hansenula saturnus* (yACCD; EC 4.1.99.2) have been well characterized (1, 10). These two kinds of ACCD perform the same activities and have amino acid sequences that are 60% identical. Although the bACCD has an estimated molecular weight that corresponds to the trimeric form of a single polypeptide chain of 338 amino acid residues, the yACCD has a molecular weight that corresponds to the dimeric form of a single polypeptide chain of 341 amino acid residues with a molecular mass of 37,500 Da (11). Both proteins have a tightly bound PLP as a cofactor per monomer. We have also purified both proteins from an overexpressing clone of *Escherichia coli* and crystallized them in earlier studies (12, 13). The crystals of yACCD are the

* This work was supported in part by Grant-in-aid for Scientific Research 11680600 from the Ministry of Education, Science, Sports and Culture, Japan. The costs of publication of this article were defrayed in part by the payment of page charges. This article must therefore be hereby marked "*advertisement*" in accordance with 18 U.S.C. Section 1734 solely to indicate this fact.

The atomic coordinates and structure factors (code 1F2D) have been deposited in the Protein Data Bank, Research Collaboratory for Structural Bioinformatics, Rutgers University, New Brunswick, NJ (http://www.rcsb.org/).

§ A member of the Sakabe Project of the Tsukuba Advanced Research Alliance (TARA), University of Tsukuba.

** To whom correspondence should be addressed. Tel.: 81-11-706-3221; Fax: 81-11-706-4905; E-mail: tanaka@castor.sci.hokudai.ac.jp.

[1] The abbreviations used are: PLP, pyridoxal 5′-phosphate; ACC, 1-aminocyclopropane-1-carboxylic acid; ACCD, 1-aminocyclopropane-1-carboxylate deaminase; yACCD, yeast 1-aminocyclopropane-1-carboxylate deaminase; bACCD, bacterial 1-aminocyclopropane-1-carboxylate deaminase; TD, threonine deaminase; OASS, *O*-acetylserine sulfhydrylase; TRPSβ, β-subunit of tryptophan synthase; MAD, multiple wavelength anomalous diffraction; PHMBS, *p*-hydroxymercuribenzene sulfonate.

more appropriate for diffraction study. Here we present the structure of the yACCD, which was determined by the multiple wavelength anomalous diffraction (MAD) method using mercury atoms as anomalous scatterers.

EXPERIMENTAL PROCEDURES

Crystallization and Data Collection—The yACCD was purified and crystallized as described previously (11, 13). Mercury derivatives of yACCD were obtained by co-crystallization with 0.5 mM *p*-hydroxymercuribenzene sulfonate (PHMBS) using the hanging drop vapor diffusion method. Two crystal forms appeared under crystallization conditions that were identical except for their protein concentrations; the orthorhombic form appeared with a protein concentration of 10 mg/ml, and the trigonal form appeared with a protein concentration of 20 mg/ml. The orthorhombic and the trigonal form diffract 2.8 and 2.5 Å resolutions, respectively.

Since only one useful mercury derivative of yACCD was found, and because non-isomorphism between the native and derivative crystals is considerable, we decided to use the MAD technique rather than the single isomorphous replacement method with anomalous scattering. The native data set of 2.0 Å and the MAD data set of 2.8 Å of the orthorhombic form were collected on the MAD beamline BM14 using a MAR imaging plate at the European Synchrotron Radiation Facility, Grenoble, France. Based on the fluorescence spectrum of the mercury atom, three different wavelengths (1.0063 Å (peak), 1.0086 Å (edge), and 0.9183 Å (remote)) were chosen for MAD phasing.

For the mercury derivative of the trigonal form, MAD data were collected at the BL18B station of Photo Factory, Tsukuba, Japan, with a Weissenberg camera (14) using two different wavelengths (1.0090 Å (edge) and 0.9800 Å (peak)), which were chosen at the L-III edge. All data sets were collected from frozen crystals at 100 K and integrated by DENZO (15). Scaling was calculated by SCALEPACK (15) for the orthorhombic form and by the CCP4 program package (16) for the trigonal form. The data collection and processing statistics are shown in Table I.

Structure Determination and Refinement—Initial phasing was carried out independently for each form of mercury derivative by MAD analysis. Because neither mercury derivative was isomorphous with the native crystals, the "remote data" and "peak data" were each treated as "native" in the orthorhombic and trigonal forms, respectively. Three of four independent mercury atoms were located in the orthorhombic form by the SHELXS (17), and two independent mercury atoms were located in the trigonal form by the RSPS (18) program. The maximum-likelihood program SHARP (19) was used for the heavy atom refinement and phasing. The initial electron density map was obtained after phase improvement by the program SOLOMON (20) implemented in SHARP (19). The operators of non-crystallographic symmetry in both forms were obtained by the program RAVE (21). The transformation matrix between the two forms was calculated by the AmoRe (22) program based on real-space molecular replacement using the two different dimer masks, which were built by the graphics program O (23).

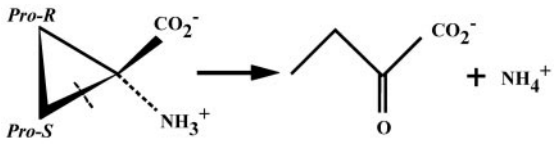

FIG. 1. **The enzymatic reaction of ACC deaminase.**

After electron density averaging of multiple crystal forms using the program RAVE (21) combined with SOLOMON (20) and the CCP4 program package (16), the atomic model was built using the baton and lego in the O program (23). Excluding two C-terminal residues, 339 out of 341 residues and the PLP cofactor were identified for each monomer on the modified electron density map. After one cycle of dynamics refinement using MAD data, the model was transferred to the native crystal by rigid body refinement at 3.0 Å, and the sigmaa (24) map was calculated as the basic map for fitting model.

Crystallographic refinement was carried out with molecular dynamics using the program CNS (25). 10% of the reflection data were set aside for the calculation of the free *R*-factor. Several cycles of simulated annealing at 3000 K, including minimization and *B*-factor refinement, were performed. In each cycle, manual model modification was carried out referring to σ-weighted ($2F_{obs} - F_{cal}$) and ($F_{obs} - F_{cal}$) maps using the program O (23). The initial structure and topology files of PLP were obtained from the Uppsala web site, HIC-Up (26). The refinement was initiated with non-crystallographic symmetry restraints. However, after several cycles of the refinement, the four monomers in the asymmetric unit showed a significant difference in the conformation at N and C termini, as well as loops between helices and β-sheets. Thus, non-crystallographic symmetry restraints were not used throughout the refinement. After 824 water molecules and a sulfoxide ion were assigned, *R*-factor and R_{free}-factor were 22.5% and 26.8% for 101,968 reflections ($F_{obs} > 3.4\sigma$, 90.3% completeness) at resolutions from 15.0 to 2.0 Å. The phasing and the refinement statistics are given in Tables II and III.

RESULTS AND DISCUSSION

Structure Description—Native yACCD was crystallized in the orthorhombic form of the space group $C222_1$ with unit cell dimensions of a = 65.7 Å, b = 268.5 Å, and c = 187.2 Å. Attempts to co-crystallize it with mercury derivatives (PHMBS) have led to two crystal forms; the first form is nearly isomorphous with the native crystals (cell dimensions are a = 65.4 Å, b = 268.3 Å, and c = 186.6 Å), and the second belongs to trigonal space group $P3_221$, with cell dimensions of $a = b$ = 79.4 Å, c = 243.6 Å, and γ = 120°. The asymmetric unit of $C222_1$ crystals contains two dimers with a solvent content of 59% (V_M = 2.98), while $P3_221$ crystals contain one dimer of yACCD in the asymmetric unit with a solvent content of 62% (V_M = 3.21). The structure of yACCD was determined by the MAD method using mercury atoms as described under "Experimental Procedures." The structure was refined against the diffraction data of native $C222_1$ crystals.

The yACCD monomer consists of two domains of different sizes. We refer to them as the small domain (residues 58–169) and the PLP-binding domain (residues 1–57 and 170–341) (Fig. 2). The secondary structure of the yACCD monomer as defined by the program DSSP (27) is shown in Figs. 3 and 5*A*. The enzyme consists of 42.8% helical (including 3_{10}-helix), 15.8% β-strand, 21.4% turn, and 20.8% unclassified coil structures. The small domain folds as an open twisted α/β structure consisting of a central four-stranded (C–F) parallel β-sheet and

TABLE I
The summary of data collection

	Native	PHMBS co-crystal form 1			PHMBS co-crystal form 2	
		Edge	Peak	Remote	Edge	Peak
Wavelength (Å)	1.0000	1.0086	1.0063	0.9183	1.0090	0.9800
Resolution (Å)[a]	100 ~ 2.0 (2.07 ~ 2.0)		100 ~ 2.8 (2.9 ~ 2.8)		20.0 ~ 2.5 (2.64 ~ 2.5)	
Space group	$C222_1$		$C222_1$		$P3_221$	
Number of observed reflections	1,000,373	391,853	386,365	381,143	128,163	123,976
Unique reflections	110,126	39,624	40,440	38,708	26,668	26,159
Completeness (%)	98.5 (96.3)	95.5 (88.4)	97.1 (85)	94.0 (92.3)	82.7 (76.7)	82.1 (76.6)
Averaged redundancy	9.08 (3.9)	9.89 (3.07)	9.55 (2.87)	9.85 (3.4)	4.8 (4.6)	4.7 (4.6)
Averaged I/σ (I)	14.6	11.1	11.9	12.6	11.1	11.0
R_{merge} (%)[b]	5.1 (22.3)	7.8 (28.1)	6.9 (24.3)	7.0 (25.3)	6.4 (23.7)	6.6 (25.3)

[a] Values in parentheses are for the outermost resolution shell.

[b] $R_{merge} = \Sigma_h\Sigma_j|\Sigma\Sigma_j<I>_h - I_{h,j}|/\Sigma_h\Sigma_j <I>_h$, where $<I>_h$ is the mean intensity of symmetry-equivalent reflections. Friedel pairs were merged as individual data.

TABLE II
The summary of phase calculation

	PHMBS co-crystal form 1			PHMBS co-crystal form 2	
Resolution (Å)		20 ~ 2.8		20.0 ~ 2.5	
Space group		$C222_1$		$P3_221$	
MAD phasing	Remote	Edge	Peak	Peak	Edge
R_{Cullis}[a]		0.598	0.601		0.438
Phasing power_iso[b]		1.426	1.139		2.397
Phasing power_ano[c]	1.124	0.964	1.189	1.925	1.427
FOM[d]		0.307			0.442
Averaging within a crystal form					
FOM		0.759			0.692
CC[e]		0.852			0.787
R-factor		30.6%			35.1%
Averaging between crystal forms					
FOM		0.804			0.813
CC		0.865			0.834
R-factor		33.3%			35.21%

[a] R_{Cullis} is the mean residual lack of closure error divided by dispersive difference. Values are for centric reflections.
[b] Phasing power_iso is the root mean square of F_H/E, where F_H is the dispersive difference of F_H and E is the lack of closure error.
[c] Phasing power_ano is as for phasing power_iso, except that F_H is the anomalous difference of F_H.
[d] FOM is the mean figure of merit.
[e] CC is standard linear correlation coefficient between observed and calculated structure factor amplitudes.

TABLE III
The final refinement statistics

Resolution range (Å)	15.0 ~ 2.0				
Number of reflections	101,968 ($F > 3.4\sigma$)				
Completeness (%)	90.38				
Total number of non-hydrogen atoms					
Protein	2607 * 4				
Others	20 * 4				
Solvent	939				
R-factor (%)[a]	22.09				
$R_{free\text{-}factor}$ (%)[b]	26.77				
r.m.s. deviation from standard values	A	B	C	D	Total
Bonds (Å)	0.006	0.006	0.013	0.011	0.010
Bond angles (degrees)	1.256	1.278	1.623	1.588	1.448
Average *B*-factor (Å^2)	A	B	C	D	Total
Main chain	51.0	55.8	25.4	28.1	40.1
Side chain	51.8	57.1	27.4	30.1	41.6
Others	45.7	54.1	21.3	21.9	33.4
Solvent					42.5
Ramachandran plot[c]	A	B	C	D	Total
Residues in most favored regions (%)	86.2	79.7	87.6	88.6	85.5
Residues in additional allowed regions (%)	13.1	19.7	11.7	11.0	13.9
Residues in generously allowed regions (%)	0.7	0.3	0.7	0.3	0.5
Residues in disallowed regions (%)	0	0.3	0	0	0.1
r.m.s. deviation (C is base) (Å)[d]	A	B	C	D	Total
Overall	0.6566	0.6775	0.0	0.6085	0.6475

[a] R-factor = $\Sigma|F_{obs} - F_{cal}|\Sigma F_{obs}$, where F_{obs} and F_{cal} are observed and calculated structure factor amplitudes.
[b] $R_{free\text{-}factor}$ value was calculated for *R*-factor, using only an unrefined subset of reflections data (10%).
[c] Anisotropic *B*-factor was calculated for overall molecule. It was applied to reflection data by CNS.
[d] Ramachandran plot was calculated by PROCHECK (35).

four surrounding helices (helices 3–6) (Fig. 2). The PLP-binding domain contains seven α-helices (helices 1, 2, and 7–11), one 3_{10}-helix 12, and six β-strands (A, B, and G–J). The core of this domain is an open twisted α/β structure with a central β-sheet surrounded by four helices (helices 7–9 and 11), similar to the small domain. The central β-sheet is basically parallel, but one terminal short strand, strand A, is antiparallel. These strands are strongly twisted so as to make the sixth strand nearly perpendicular to the first. There is a crevice at the carboxyl ends of the β-strands G and J, which makes a space for bound PLP. Except for α-helices 2 and 10, all α-helices of the two domains have a chain direction toward the molecular surface, and all β-strands are directed toward the molecular center. The 3_{10}-helix 12 at the C terminus consists of 11 residues with a kink in the middle. The 3_{10}-helix is energetically unfavorable, and only short pieces are found in protein structures. The kinked 3_{10}-helix of yACCD is at the interface region between two domains. The two domains are connected by two linkers (residues 56–58 and 162–173). Between the two domains, there is a large internal gap of 5.8 Å × 6.8 Å × 12 Å that includes the crevice mentioned above. This large internal gap provides a space for the active site (Fig. 2).

Two monomers of yACCD interact closely with each other at their nearly flat surfaces, forming a dimer with a dyad axis running through the interacting surfaces (Figs. 4 and 5*B*). The interface between the two monomers is formed through hydrogen bonds and hydrophobic interactions. The buried accessible surface area between the two monomers is 14.0% of the total molecular accessible surface (calculated by the CNS program (Ref. 25)). The monomer-monomer contacts involve 18 pairs of hydrogen bonds by 17 residues (Arg^{23}–Ala^{89}, Arg^{38}–Gly^{44}, Ala^{46}–Gly^{288}, Ala^{89}–Gln^{286}, Arg^{115}–Ser^{333}, Val^{117}–Ser^{330}, Glu^{120}–Leu^{329}, Arg^{123}–Thr^{338}, and Gly^{126}–Lys^{339} and their dyad symmetry mates), and 22 pairs of van der Waals contacts by 18 residues (Phe^{13}–Pro^{17}, Leu^{45}–Glu^{287}, Phe^{47}–Phe^{47}, Phe^{47}–Ala^{326}, Ala^{89}–Ala^{284}, Ala^{89}–Glu^{285}, Glu^{120}–Ser^{333}, Leu^{121}–Leu^{290}, Ile^{124}–Ala^{284}, Ile^{124}–Phe^{336}, Asp^{128}–Ala^{341}, and their dyad symmetry mates). At the center of the monomer-

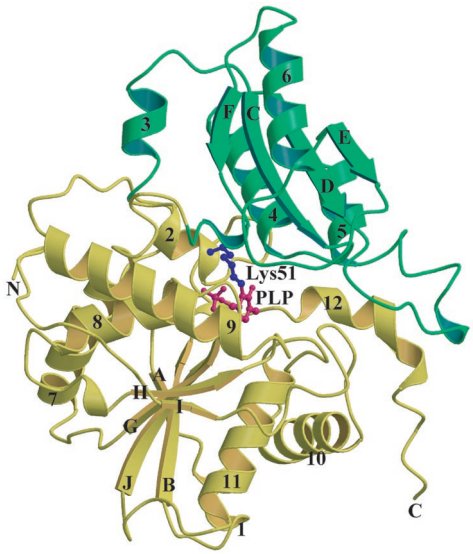

FIG. 2. **Ribbon diagram of the yACCD monomer consisting of two domains.** *Green* represents the small domain (residues 58–169), and *yellow* represents the PLP-binding domain (residues 1–57 and 170–341). Both domains fold as an open twisted α/β structure consisting of a central β-sheet and surrounding helices. The PLP molecule (*red*) and Lys^{51} (*blue*) are shown as *ball-and-stick*.

monomer interface, a hydrophobic core is formed by five hydrophobic residues from both monomers: Phe^{47}, Leu^{121}, Leu^{290}, Pro^{327}, and Ala^{326}. Most of the residues involved in the contacts are at helices 1, 4, and 12 of the N and C termini. The tightly bound dimer may contribute to the stability of the yACCD.

Crystal Packing—Two crystallographically independent dimers (AB and CD) of yACCD have different packing interactions in the crystal; the CD dimer has more extensive interactions with five symmetry-related CD dimers and two symmetry-related AB dimers, while the AB dimer has contact with four symmetry-related AB dimers and two symmetry-related CD dimers. Because of this obvious difference in the environment in the crystal, the features of the electron densities in the two types of dimers were significantly different; the electron density in the AB dimer was poor in parts. Therefore, the number of water molecules assigned through the refinement were also different: 685 for the CD dimer and 254 for the AB dimer. Main-chain temperature factors of the two crystallographically independent dimers were also significantly different (Table III). The AB and CD dimers were also related by the pseudo-dyad axis. However, this axis was not perpendicular to the individual dimer axis, and the interactions between the two dimers were weak.

Comparisons with Other PLP-dependent Enzymes—Three-dimensional structure comparisons were carried out using the program DARI (28) with entries from the Protein Data Bank (29) in order to search for all of the related structures. Among all of the PLP-dependent enzymes that have been published in the Protein Data Bank, the β-subunit of tryptophan synthase from *Salmonella typhimurium* (TRPSβ) (30), *O*-acetylserine sulfhydrylase from *S. typhimurium* (OASS) (31), and threonine deaminase from *E. coli* (TD) (32) have some similarity to yACCD (Fig. 5*B*). All of these molecules belong to the β family of the PLP-dependent enzymes (6). It has been previously suggested that the PLP-binding regions in these enzymes share the same fold, which consist of two domains (33). Some of the earliest descriptions of the structural attributes of yACCD based on a sequence comparison with TRPSβ (16% identities in sequences) also suggested that the fold of yACCD would bare some similarity to that of TRPSβ (11). On the other hand, the sequence comparisons of yACCD with TD and OASS detected (if any) very limited similarity (Fig. 3). The TRPSβ was the first member of the β family of the PLP-dependent enzymes to have its three-dimensional structure determined by x-ray crystallography (30). Tryptophan synthase exists as an $\alpha\beta\beta\alpha$ type tetramer with a dyad axis between the two β subunits. TD is the allosteric enzyme that exists as a homotetramer with 222 symmetry. Each monomer of TD contains one catalytic domain (the PLP-binding domain) and one regulatory domain. The catalytic domain of TD is structurally similar to yACCD. OASS is a dimeric molecule with a dyad axis at the center.

Although the chemistries involved in these enzymatic reactions and quaternary association are different (two of the four members are tetramers), the overall folding topologies of these molecules are clearly related each other (Fig. 5*A*). Also, the dimer interface is more or less conserved in the four enzymes (Fig. 5*B*). A careful comparison of the tertiary structures and folding topologies of these molecules reveals several important regions in the enzymes. The largest difference in the folding topology of ACCD and other members in the β family of the PLP-dependent enzymes is at helix 9. In three other members (TRPSβ, TD, and OASS), helix 9 of ACCD is replaced by a region consisting of a long loop and helices (Fig. 5*A*). This inserted region makes close contact with the *re* face of PLP and may be important for positioning the PLP at an appropriate place for adapting to each substrate. This inserted region is actually one of the most diverted regions in these three enzymes. Although ACCD does not contain this region, the PLP is nonetheless exposed to the molecular surface due to the presence of a loop between strand I and helix 10 (residues 262–273) and two extra loops mentioned in the following section. Topologically, the folding of ACCD is the simplest and probably represents a more ancient fold in this family of proteins.

Coenzyme Binding Site—As a typical open twisted α/β structure, the PLP cofactor is positioned at a crevice between the β-strands (G and J) of the PLP-binding domain and lies on the large internal gap between the two domains (Fig. 2). The PLP cofactor is covalently bound through a Schiff base linkage to NZ of Lys^{51} with C4′ (the internal aldimine) (Fig. 6). This mode of binding is consistently observed in the PLP-dependent enzymes. However, the environments surrounding PLP are fairly different from those of other PLP-dependent enzymes. The *re* side of the internal aldimine of the β family of PLP-dependent proteins, whose tertiary structures have been determined, faces the active-site entrance and is open. At the front side of the PLP pyridine of the yACCD, however, the three extra loops bury the PLP deep in the interior of the molecule (Fig. 7). These are the loops between strand D and helix 5 (residues 101–116), and between strand E and helix 6 (residues 132 and 141) in the small domain, and the loop between strand I and helix 10 (residues 262–273) in the PLP-binding domain.

Behind these loops, two cavities with different sizes were formed, as calculated by VOIDOO (34) of the Uppsala program package and the MS[2] program (Fig. 7). The small (inner diameter, 3.2 × 7.5 Å) one is located along the direction of the substrate tunnel of the tryptophan synthase. The residues Arg^{240}, Gln^{237}, and Gln^{167} are positioned at the entrance. However, this cavity does not pass through to the active center without a movement of the peptide chain, since Ala^{163} and Thr^{202} (CB of Ala^{163} and OE of Thr^{202}) close the gate to the active center. The large cavity has an inner diameter size of ϕ3.0 × 18.2 Å, including the substrate area. The cavity links the active center to the surface of the molecule along a loop between strand C and helix 4. The walls of these cavities are formed mostly by aromatic residues (Trp^{102}, Tyr^{113}, Tyr^{269}, and

[2] C. P. Libeu, unpublished result.

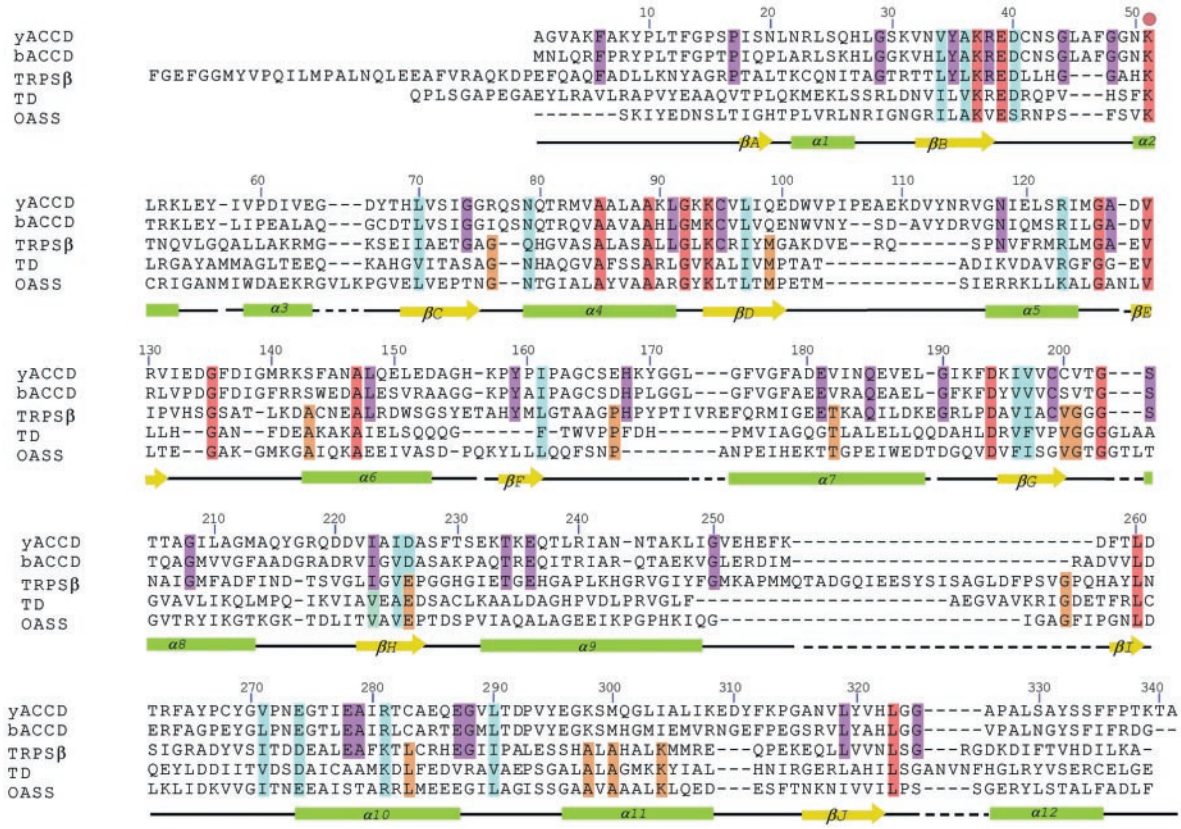

FIG. 3. **Sequence alignment of ACCDs and the β family of PLP-dependent enzymes.** The sequences displayed are yACCD (from yeast *H. saturnus*), bACCD (from *Pseudomonas sp.*), TRPSβ (30) (from *S. typhimurium*), TD (32) (from *E. coli*), and OASS (31) (from *S. typhimurium*). The sequence of yACCD has 17% identity to TRPSβ but has very low (if any) identity to TD or OASS. However, the sequences of the latter two have more similarity to TRPSβ. The amino acid residues are shaded as follows: completely identical (*red*), conserved change (*light blue*), first three are identical (*purple*), last three are identical (*light brown*). The *star* represents the Lys residue to which PLP is bound. The secondary structure elements indicated are those defined by the present work for the yACCD, using the program DSSP (27).

Tyr^{295}) and hydrophobic residues (Val^{103}, Ile^{138}, and Val^{294}). These aromatic and hydrophobic residues favor the formation of hydrophobic environments for the enzymatic reaction and of a tight channel for substrate/product transportation.

A more detailed inspection of the structure around the PLP revealed further differences between this enzyme and other members of the β family of the PLP-dependent proteins. In three other members of the β family of the PLP-dependent proteins, the residues immediately preceding PLP-bound Lys are aromatic or bulky hydrophobic, such as His^{86} of TRPSβ (30), Phe^{61} of TD (32), and Val^{40} of OASS (31). These residues may function to prevent a backward tilt of the coenzyme pyridine ring (31). In the case of ACCD, the Asn^{50} immediately preceding Lys^{51} is involved in the hydrogen-bonding network mediated by water molecules (Fig. 8). This residue and Leu^{323} are close to the PLP and seem to play a role in supporting the pyridinium plane from the backside. The front side (*re* face) is also different from other members of the β family of PLP-dependent proteins. The phenol group of Tyr^{295} is stacked to the plane of the pyridinium ring with a distance of 3.9 Å, and an angle of about 20° (Fig. 6). Although this is the first observation of such stacking in the β family of the PLP-dependent proteins, the stacking of two rings has been found in other types of PLP-dependent enzymes (36–38). This finding may represent convergent evolutions, since the sequence comparison suggested that there is no evolutionary relationship between the β family and other types of PLP-dependent enzymes (6). As discussed in a previous study, the stacking structure favors the formation of the quinonoid intermediate (39).

The N1 nitrogen (pyridinium N) of the cofactor pyridine ring is within hydrogen bonding distance of the OE1 of Glu^{296}. This

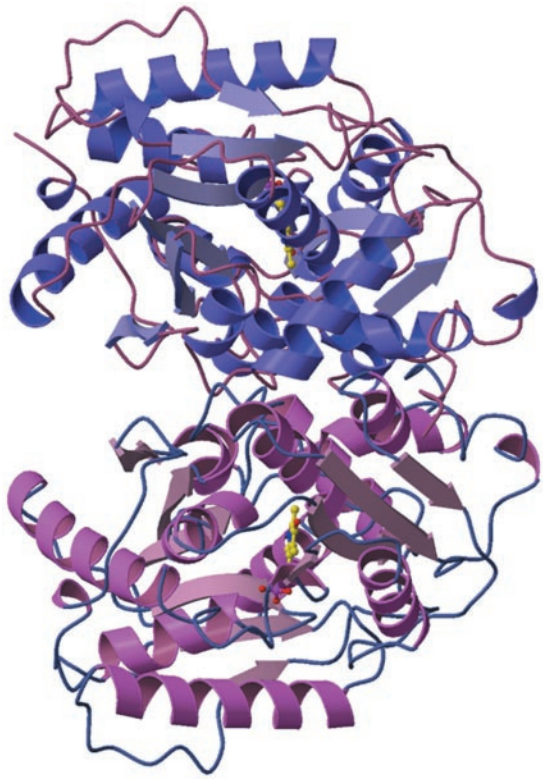

FIG. 4. **Ribbon diagram of yACCD dimer.** A two-fold axis runs from the *left* to the *right*. The viewing points of this figure and Fig. 5*A* are orthogonal to each other.

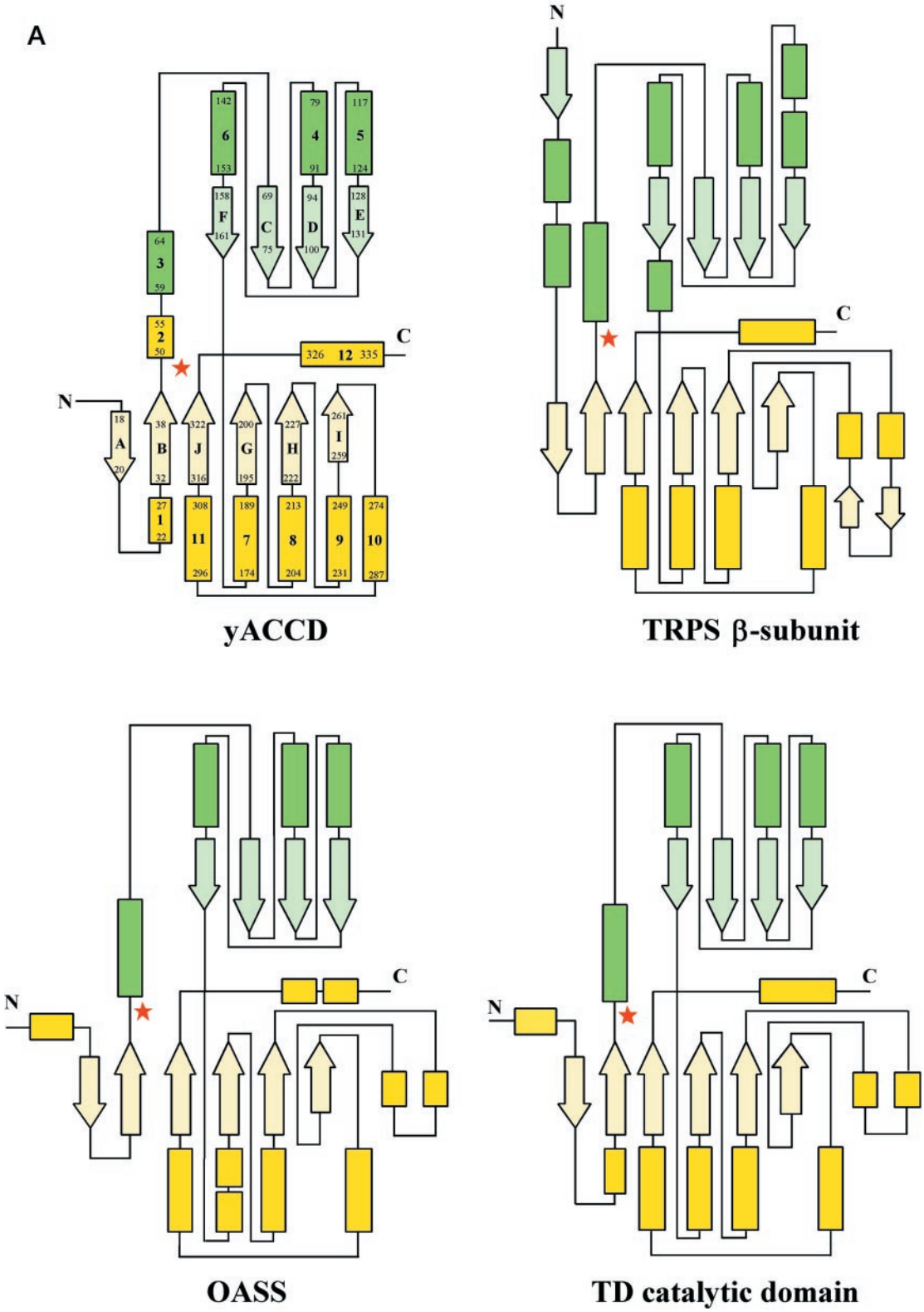

FIG. 5. **Comparison of the β family of PLP-dependent enzymes.** The abbreviations are explained in Fig. 3. *A*, comparison of the folding topology of the β family of the PLP-dependent enzymes. The *rectangles* represent the α-helix, and *arrows* represent the β-strand. The *red star* is the position of the Lys residue to which PLP is bound. *b*, ribbon representation of the dimer molecules viewed from the two-fold axis. In case of TD (32), regulatory domains (data not shown) have stronger interactions; thus, the interactions of the catalytic domains are weak. Molecules are drawn in the colors changing from the N-terminal *blue* to the C-terminal *red*.

position is occupied by Ser in three other members of the β family of PLP-dependent enzymes whose tertiary structures have been determined. Since Glu^{296} is negatively charged, it stabilizes the positively charged PLP, thereby increasing the electron-withdrawing properties of the cofactor. OE1 of Glu^{296} also forms strong hydrogen bonds to the main-chain nitrogen atom of Ile^{323} and to a water molecule (Fig. 8). The O3′ of the cofactor is in close contact with the side chain of Asn^{79}, which also forms strong hydrogen bonds to ND of Asn^{118} and to NH of Arg^{82}. Moreover, OD of Asn^{50} is involved in a hydrogen-bond-

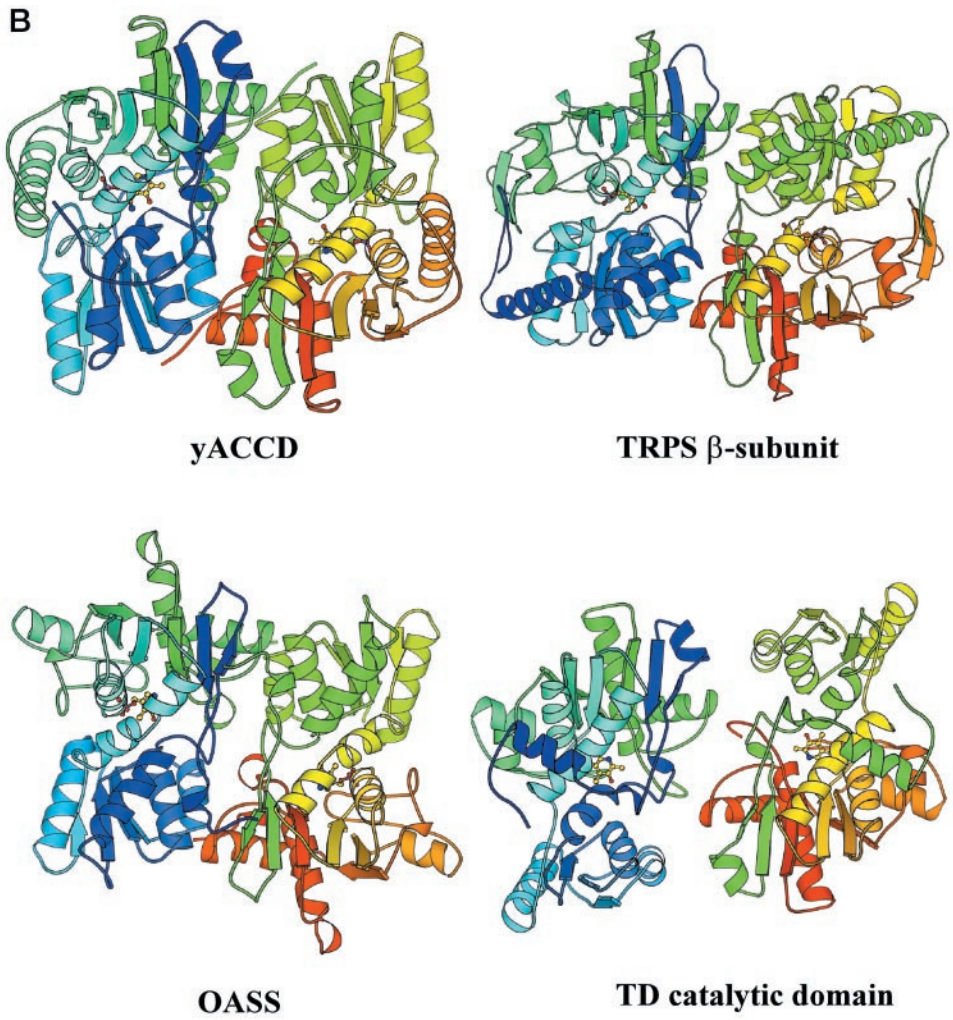

FIG. 5—*continued*

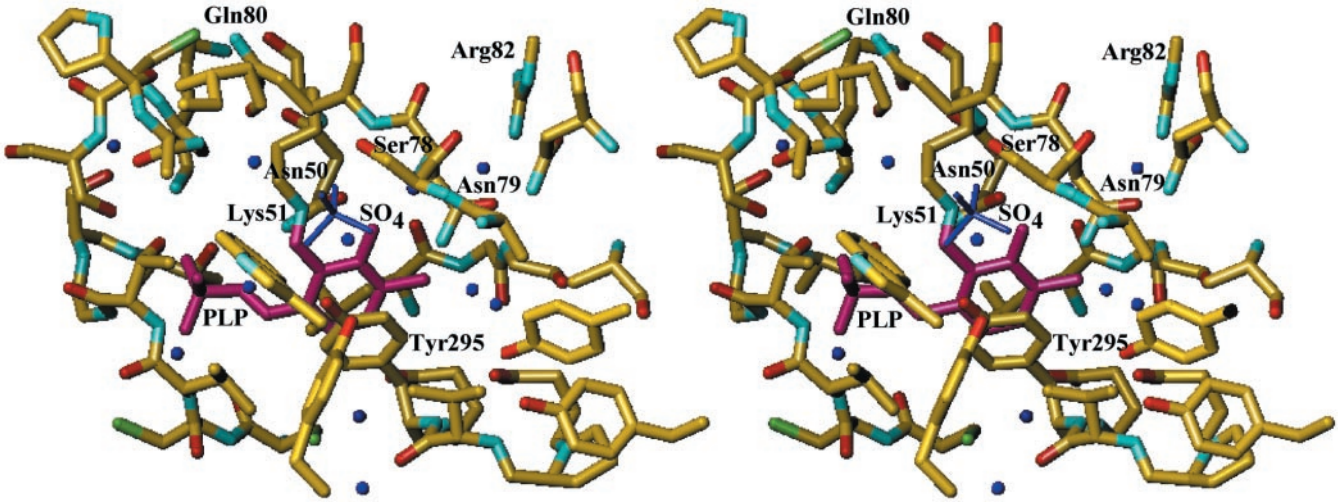

FIG. 6. **A stereoscopic view of the active site region of yACCD.** The PLP cofactor (drawn in *wine color*) is covalently bound in Schiff base linkage to NZ of Lys^{51} with C4′ (the internal aldimine). The environments surrounding PLP are fairly different from those of other PLP-dependent enzymes (30–32). The *re* face of the cofactor is stacked to the plane of phenol group of Tyr^{295} with a distance of 3.9 Å and an angle of about 20°. The bound sulfoxide ion is also drawn in *blue wire*, and water molecules are drawn as *blue spheres*.

ing network to O3′ of the cofactor via a bridged water molecule. These hydrogen bonds would impede any rotation of these residues and allow charge dissipation over the hydrogen network.

Despite these major differences in the cofactor binding, these enzymes have a common recognition mechanism as well. The phosphate group of PLP was tightly fixed in a pocket formed by the residues Lys^{54}, Val^{201}, Thr^{202}, Gly^{203}, and Thr^{205} with their hydrogen bonding networks around the loop region between β-strand G and helix 8 (Fig. 8). Val^{201} and Gly^{203} made hydro-

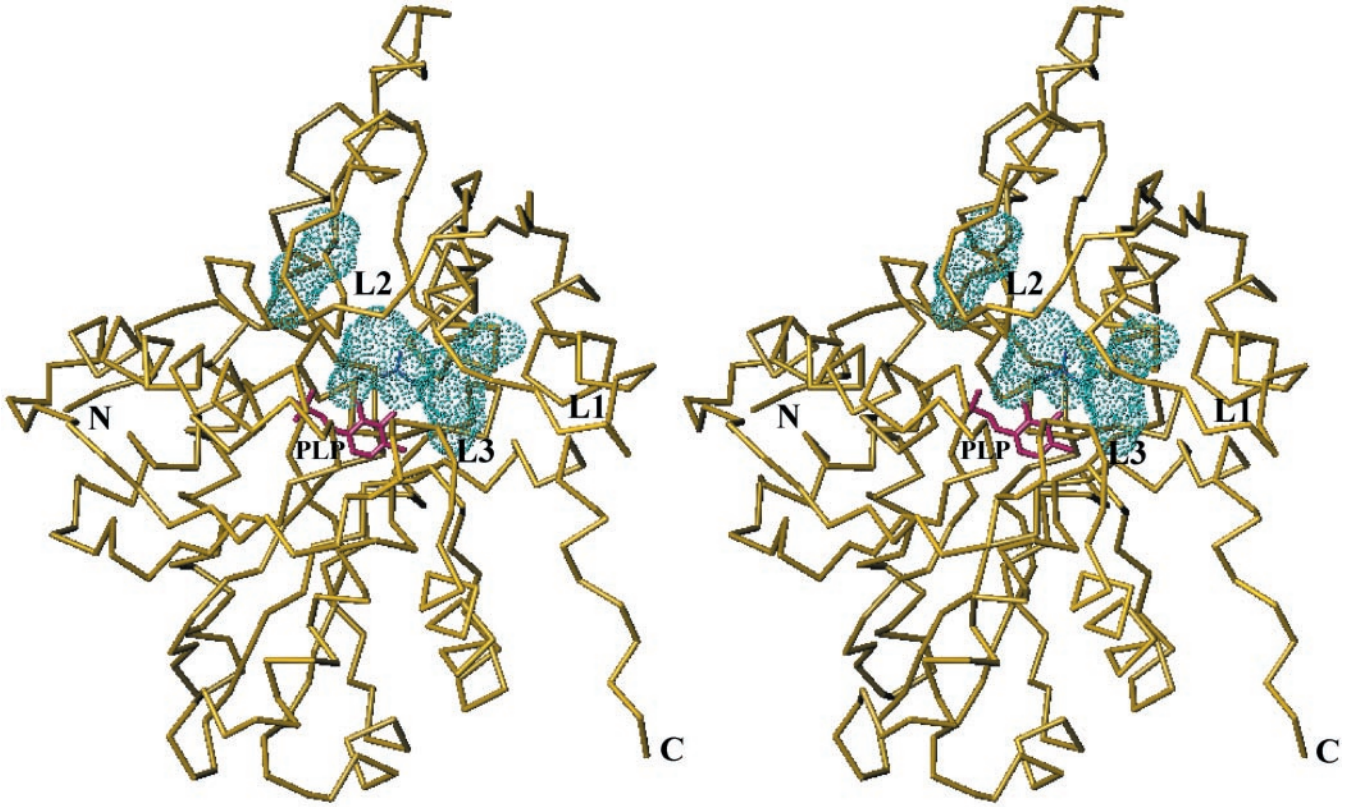

FIG. 7. **A stereoscopic drawing of yACCD monomer showing buried PLP (*red*).** Unlike other members of the β family of the PLP-dependent enzymes, the PLP of yACCD is buried deep in the interior of the molecule by the three characteristic loops marked by *L1* (the loop between strand D and helix 5), *L2* (the loop between strand E and helix 6), and *L3* (the loop between strand I and helix 10). Calculated cavities, which may be important for the enzymatic reaction and for substrate/product transportation, are drawn as *blue-dotted* surfaces.

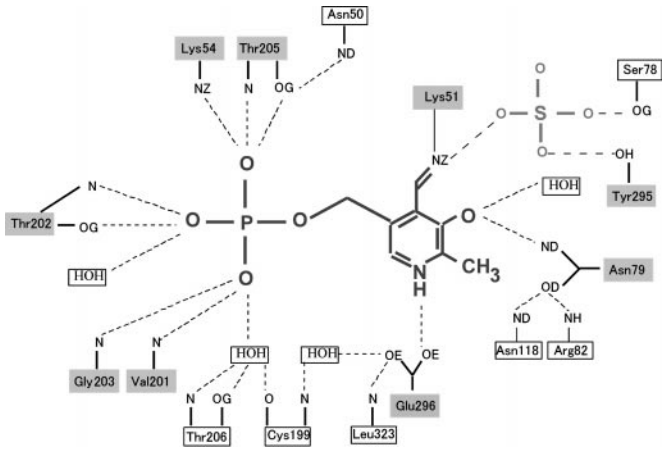

FIG. 8. **Hydrogen bonding networks around the active site.**

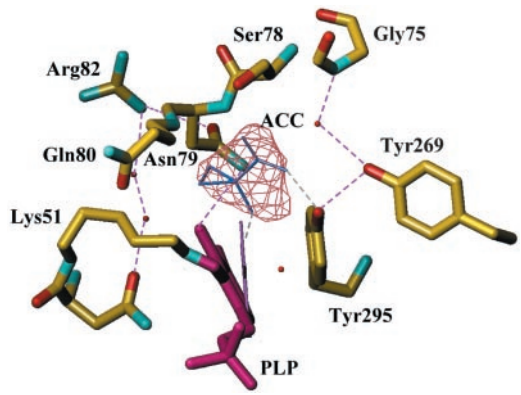

FIG. 9. **A detailed view of the PLP-binding site and proposed substrate complex.** ACC is modeled on the electron density for the bound sulfoxide ion. *Thin bonds* are hypothetical drawings of PLP and the bound substrate (see "Reaction Mechanism").

gen bonds to the Op2 via their main-chain nitrogen atoms. There was a water molecule located between Op2 and Cys^{199}/Thr^{206} within hydrogen-bonding distance. The three hydrogen bonds of Op3 were formed by N and OG of Thr^{202} and a water molecule. There were three hydrogen bonds between Op1 and NZ of Lys^{54}, and between N and OG of Thr^{205}. These environments of the phosphate group-binding pocket are conserved in three other PLP-dependent enzymes of the β family (TRPSβ, TD, and OASS).

Reaction Mechanism—An earlier experiment showed that ACC deaminase opens the cyclopropane ring at a bond between α carbon and *pro-S* methylene carbon (Fig. 1) (40). Furthermore, ACC deaminase showed reactivity toward D-amino acids such as D-alanine and D-serine (but not L-isomers) (8), which suggested the presence of a base at the active site for the removal of a proton from the α carbon of the D-amino acid. Previous chemical and genetic studies have also implicated residues that contribute to catalysis. The enzymatic activity of ACCD is inhibited by modifying Cys^{162} of bACCD (which corresponds to Cys^{165} of yACCD) with sulfhydryl-modifying reagents (41). However, further experiments have shown that substitution of this residue to Ala does not affect the enzymatic activity, suggesting that Cys^{165} is not directly involved in the enzymatic activity (42). On the other hand, the replacement of Lys^{51} with Ala at the PLP-binding site caused a loss of detectable ACC deamination activity (42). The present structure analysis is consistent with these earlier observations. Cys^{162} is positioned at the internal gap between the two domains. The chemical modification by the bulky reagents may have altered

the relative orientation of the two domains, thereby causing the loss of enzymatic activity.

Although the crystals of yACCD were grown without any substrates or inhibitors, the present analysis has shown an important clue to the enzymatic reaction mechanism, namely that the electron density map (with phases calculated by MAD and density modification) or the difference Fourier map revealed a significant peak with a trigonal bipyramid shape that could be interpreted to be a sulfoxide or phosphorous ion (Fig. 9). This is the largest peak in the difference Fourier map. The position of the peak is close to the PLP and within hydrogen-binding distance of the OG of Ser^{78}, OH of Tyr^{295}, N of Gln^{80}, and N of Asn^{79}. It is thus very likely that the substrate pocket is occupied by the sulfoxide or phosphorous ion in the crystallization buffer. A model of the substrate ACC was built into the peak position of the electron density map using the graphical software O (23). In order to form an external aldimine between the ACC and PLP, the PLP should be rotated by about 20° where the pyridinium ring of PLP is parallel to the phenol group of Tyr^{295} (Fig. 9). The resulting complex structure suggests that Tyr^{295} at the *re* side of the PLP may play a role in binding the substrates by the hydrogen bond.

The reaction mechanism of the ACCD was studied previously by NMR method using modified substrates including cyclic and acyclic substrates. Such studies have suggested two mechanistic routes: 1) a nucleophilic attack on *pro-S* to cleave the bond between *pro-S* and Cα of ACC followed by the abstraction of proton from *pro-R* (nucleophilic route), 2) direct *pro-S*-proton abstraction to initiate the cyclopropane ring fragmentation (direct abstraction route) (8). The first route is more likely because the second route requires abstraction of an inert proton from the ring for initial reaction and such an anion-induced ring cleavage is stereoelectronically unfavored (9). In the light of these previous descriptions, we sought for the residues that are involved in the enzymatic reaction. Although no clear-cut reaction mechanism could be proposed from the present analysis alone, the most likely candidate for the nucleophile is Ser^{78}. This residue is hydrogen-bonded to Thr^{81} and is close to the putative ACC molecule. In this case, the released Lys^{51} is the most likely candidate for base for proton abstraction. In order to clarify such reaction mechanism, the site-directed mutagenesis studies are currently under way.

Acknowledgments—We thank A. Thompson and V. Stojanoff of the European Synchrotron Radiation Facility (Grenoble, France) and N. Sakabe, N. Watanabe, M. Suzuki, and N. Igarashi of the Photon Factory, National Laboratory for High Energy Physics (Tsukuba, Japan), for their kind help during data collection. We also thank S. Aimoto at the Institute for Protein Research (Suita, Japan) for valuable comments.

REFERENCES

1. Honma, M., and Shimomura, T. (1978) *Agric. Biol. Chem.* **42,** 1825–1831
2. Burroughs, L. F. (1957) *Nature* **179,** 360–361
3. Adams, D. O., and Yang, S. F. (1979) *Proc. Natl. Acad. Sci. U. S. A.* **76,** 170–174
4. Klee, H. J., Hayford, M. B., Kretzmer, K. A., Barry, G. F., and Kishore, G. M. (1991) *Plant Cell* **3,** 1187–1193
5. Reed, A. J., Kretzmer, K. A., Naylor, M. W., Finn, R. F., Magin, K. M., Hammond, B. G., Leimgruber, R. M., Rogers, S. G., and Fuchs, R. L. (1996) *J. Agric. Food Chem.* **44,** 388–394
6. Alexander, F. W., Sandmeier, E., Mehta, P. K., and Christen, P. (1994) *Eur. J. Biochem.* **219,** 953–960
7. John, R. A (1995) *Biochim. Biophys. Acta* **1248,** 81–96
8. Walsh, C., Pascal, R. A., Jr., Johnston, M., Raines, R., Dikshit, D., Krantz, A., and Honma, M. (1981) *Biochemistry* **20,** 7509–7519
9. Li, K., Du, W., Que, N. L. S., and Liu, H. W. (1996) *J. Am. Chem. Soc.* **118,** 8763–8764
10. Sheehy, R. E., Honma, M., Yamada, M., Sasaki, T., Martineau, B., and Hiatt, W. R. (1991) *J. Bacteriol.* **173,** 5260–5265
11. Minami, R., Uchiyama, K., Murakami, T., Kawai, J., Mikami, K., Yamada, T., Yokoi D., Ito, H., Matsui, H., and Honma, M. (1998) *J. Biochem.* (*Tokyo*) **123,** 1112–1118
12. Yao, M., Tanaka, I., and Honma, M. (1994) *J. Struct. Biol.* **113,** 251–253
13. Yao, M., Horiuchi, A., Tanaka, I., and Honma, M. (1995) *Protein Peptide Lett.* **2,** 305–306
14. Sakabe, N. (1991) *Nucl. Instrum. Methods* **303,** 448–463
15. Otwinowski, Z., and Minor, W. (1997) *Methods Enzymol.* **276,** 307–32
16. Collaborative Computational Project, Number 4 (1994) *Acta Crystallogr. Sect. D Biol. Crystallogr.* **50,** 760–763
17. Sheldrick, G. M., Dauter, Z., Wilson, K. S., Hope, H., and Sieker, L. C. (1993) *Acta Crystallogr. Sect. D Biol. Crystallogr.* **49,** 18–23
18. Knight, S. (1989) *Ribulose 1.5-Bisphosphate Carboxylase/Oxygenase—A Structural Study.* Ph.D. thesis, Swedish University of Agricultural Sciences, Uppsala, Sweden
19. De La Fortelle, E., and Bricogne, G. (1997) *Methods Enzymol.* **276,** 472–494
20. Abrahams, J. P., and Leslie, A. G. W. (1996) *Acta Crystallogr. Sect. D Biol. Crystallogr.* **52,** 30–42
21. Kleywegt, G. J., and Read, R. J. (1997) *Structure* **5,** 1557–1569
22. Navaza, J. (1994) *Acta Crystallogr. Sect. A* **50,** 157–163
23. Jones, T. A., Zou, J. Y., Cowan, S. W., and Kjeldgaard, M. (1991) *Acta Crystallogr. Sect. A* **47,** 110–119
24. Read, R. J. (1986) *Acta Crystallogr. Sect. A* **42,** 140–149
25. Brünger, A. T., Adams, P. D., Clore, G. M., Delano, W. L., Gros, P., Grosse-Kunstleve, R. W., Jiang, J.-S., Kuszewski, J., Nilges, N., Pannu, N., S., Read, R. J., Rice, L. M., Simonson, T., and Warren, G. L., (1998) *Acta Crystallogr. Sect. D Biol. Crystallogr.* **54,** 905–921
26. Kleywegt, G. J., and Jones, T. A. (1998) *Acta Crystallogr. Sect. D Biol. Crystallogr.* **54,** 1119–1131
27. Kabsch, W., and Sander, C. (1983) *Biopolymers* **22,** 2577–2637
28. Holm, L., and Sander, C. (1996) *Science* **273,** 595–560
29. Abola, E. E., Sussman, J. L., Prilusky, J., and Manning, N. O. (1997) *Methods Enzymol.* **276,** 556–571
30. Hyde, C. C., Ahmed, S. A., Padlan, E. A., Miles, E. W., and Davies, D. R. (1988) *J. Biol. Chem.* **263,** 17857–17871
31. Burkhard, P., Rao, G. S. J., Hohenester, E., Schnackerz, K. D., Cook, P. F., and Jansonius, J. N. (1998) *J. Mol. Biol.* **283,** 121–133
32. Gallagher, D. T., Gilliland G. L., Xiao, G., Zondlo, J., Fisher, K. E., Chinchilla, D., and Eisenstein, E. (1998) *Structure* **6,** 465–475
33. Schneider, G., Kaeck, H., and Lindqvist, Y. (2000) *Structure* **8,** R1–R6
34. Kleywegt, G. J., and Jones, T. A. (1994) *Acta Crystallogr. Sect. D Biol. Crystallogr.* **50,** 178–185
35. Laskowski, R. A., Mac Arthur, M. W., Moss, D. S., and Thornton, J. M. (1993) *J. Appl. Crystallogr.* **26,** 283–291
36. Ford, G. C., Eichele, G., Jansonius, J. N. (1980) *Proc. Natl. Acad. Sci. U. S. A.* **77,** 2559–2563
37. Kern, A. D., Oliveira, M. A., Coffino, P., and Hackert, M. L. (1999) *Structure* **7,** 567–581
38. Clausen, T., Schlegel, A., Peist, R., Schneider, E., Steegborn, C., Chang, Y. S., Haase, A., Bourenkov, G. P., Bartunik, H. D., and Boos, W. (2000) *EMBO J.* **19,** 831–842
39. Dunathan, H. C. (1966) *Proc. Natl. Acad. Sci. U. S. A.* **55,** 712–716
40. Honma, M., Shimomura, T., Shiraishi, K., Ichihara, A., and Sakamura, S. (1979) *Agric. Biol. Chem.* **43,** 1677–1679
41. Honma, M. (1985) *Agric. Biol. Chem.* **49,** 567–571
42. Murakami, T., Kiuchi, M., Ito H., Matsui H., and Honma M. (1997) *Biosci. Biotech. Biochem.* **61,** 506–509

Crystal Structure of 1-Aminocyclopropane-1-carboxylate Deaminase from *Hansenula saturnus*

Min Yao, T. Ose, Hiroshi Sugimoto, Atsushi Horiuchi, Atsushi Nakagawa, Soichi Wakatsuki, Daisuke Yokoi, Toyotaka Murakami, Mamoru Honma and Isao Tanaka

J. Biol. Chem. 2000, 275:34557-34565.
doi: 10.1074/jbc.M004681200 originally published online August 10, 2000
